



Dominance of Shape Anisotropy among Magnetostatic Interaction and Magnetocrystalline Anisotropy in Electrodeposited $(\text{FeCo})_{1-x}\text{Cu}_x$ ($X = 0.1-0.5$) Ternary Alloy Nanowires

Naeem Ahmad^{1,2} · M. Zahid Shafiq¹ · Suleman Khan¹ · Wiqar Hussain Shah¹ · Imran Murtaza¹ · Abdul Majid³ · Khalid Javed⁴

Received: 18 October 2019 / Accepted: 3 December 2019 / Published online: 17 December 2019
© Springer Science+Business Media, LLC, part of Springer Nature 2019

Abstract

The $(\text{FeCo})_{1-x}\text{Cu}_x$ ($X = 0.1-0.5$) nanowire (NWs) arrays were synthesized through AC-electrochemical deposition in anodized aluminum oxide (AAO) templates. The morphology and composition of the synthesized (FeCoCu) NWs were found from scanning electron microscope (SEM), and energy dispersive X-ray spectroscopy (EDS) that confirmed the diameter of the NWs is in the range of 50–60 nm and the composition of FeCoCu alloy NWs, respectively. The XRD measurement of the NWs was carried out in AAO templates along with Al-substrate. The FeCoCu alloy NWs show BCC phase along with reflection peak (311) in all samples which corresponds to Al-substrate. The crystallite size displays overall increasing trend confirmed through XRD using Scherrer equation. The magnetic analysis reveals that by increasing the Cu concentration in FeCoCu alloy NWs, the saturation magnetization and coercivity (H_c) decreased. The results of MH loops confirmed that easy axis lies along the NWs and hard axis perpendicular to the NWs due to dominance of shape anisotropy. Magnetization reversal mechanism occurs by nucleation mode with the motion of domain walls. The frequency-dependent dielectric analysis investigated thoroughly using impedance and the behavior of dielectric parameters has been examined using Maxwell-Wagner's model and Koop's theory. The value of dielectric constant decreases progressively with increasing frequency and vice versa. It is also observed that with increase in Cu concentration, the dielectric constant also decreases due to higher conductivity of Cu than Fe and Co.

Keywords Anodized aluminum oxide templates · FeCoCu nanowires · Magnetization reversal · Shape anisotropy and magnetostatic interactions

1 Introduction

The nanostructures based on template fabrication have fascinated and provided facilities to researchers working in material science to fabricate nanostructures such as nanotubes, nanoparticles, and nanowires (NWs) which show

optical, electrical, and magnetic properties different from their bulk counterpart. Applications of ferromagnetic NWs are in optical medium, electronic equipment, and dense magnetic memories [1, 2]. Ferromagnetic NWs arrays also have applications in nanosensors [3] and magnetic nanodevices [4] recording media [5], and even micro circulator of magnetic NWs is attracting a lot of attention [6]. The synthesis of magnetic NWs arrays into self-assembled nanoporous templates is a versatile technique to prepare nanomaterials. The geometrical parameters of nanoporous templates like pore length, diameter, and interpore distance can be controlled by changing the time of anodization, applied potential, and temperature of acidic solution, respectively. In this way, highly ordered and uniform nanoporous templates with length ranging from 100 to 50 μm and diameter from 15 to 200 nm can be easily obtained. Since the last decade, binary ferromagnetic

✉ Naeem Ahmad
naeem.ahmad@iiu.edu.pk

¹ Spintronics Laboratory, Department of Physics, FBAS, International Islamic University, Islamabad 44000, Pakistan

² Beijing National Laboratory for Condensed Matter Physics, Institute of Physics, University of Chinese Academy of Sciences (UCAS), Beijing 100190, China

³ Department of Physics, University of Gujrat, Gujrat, Pakistan

⁴ Department of Physics, FC College University, Lahore, Pakistan

nanowire arrays with nonmagnetic element like CoAg, FeAg, CoPt, CoPd, and CoCu have been the focus of researchers due to its motivating, promising, interesting magnetotransport and magnetic properties [7–9].

FeCo NWs show the capability to synthesize the formation of permanent magnet among various binary alloy systems. Furthermore, the structural, magnetic, and dielectric properties can be tuned through varying the composition of $(\text{FeCo})_{1-x}\text{Cu}_x$ alloy NWs [10, 11], or proper heat treatment [11]. Specially, due to higher value of shape anisotropy in NWs, higher values of coercivity and remanence are expected along the NWs long axis [12, 13]. Fabrication of FeCoCu NWs into AAO templates by AC electrodeposition is very difficult due to mismatch of reduction potential and difference of ionic radii. It is required to enhance the magnetic properties of FeCo alloy NWs and discuss magnetization reversal process to be employed in high density recording media and magnetic race track memory [14–19].

After the preparation of all samples, they were characterized/investigated through various techniques such as Fourier transform infrared spectroscopy (FTIR), X-ray diffraction (XRD), scanning electron microscopy (SEM), energy

dispersive X-ray (EDX) spectroscopy, LCR meter, and vibrating sample magnetometer (VSM).

2 Experimental Details

2.1 Template Fabrication

Recently, we have synthesized AAO templates [13, 14] using two steps of anodization. For such purpose, we took aluminum (99.99%) sheet that was first annealed at 500 °C to obtain homogenous pore growth conditions. Then, Al sheet was electro-polished in the ratio of 1:4 of HClO_4 and $\text{C}_2\text{H}_5\text{OH}$, respectively, at 9 V (DC) to reduce the surface roughness. Afterward, the first anodization of pre-treated Al sheet was formed in 5% H_3PO_4 acid at 60 V DC for 6 h, and during anodization, temperature of electrolyte was kept constant stirring continuously. Then, the anodized foils were immersed into mixture solution of 6 wt% H_3PO_4 and 1.8 wt% CrO_3 at 60 °C for 2 h to remove the formed anodized layer because it has

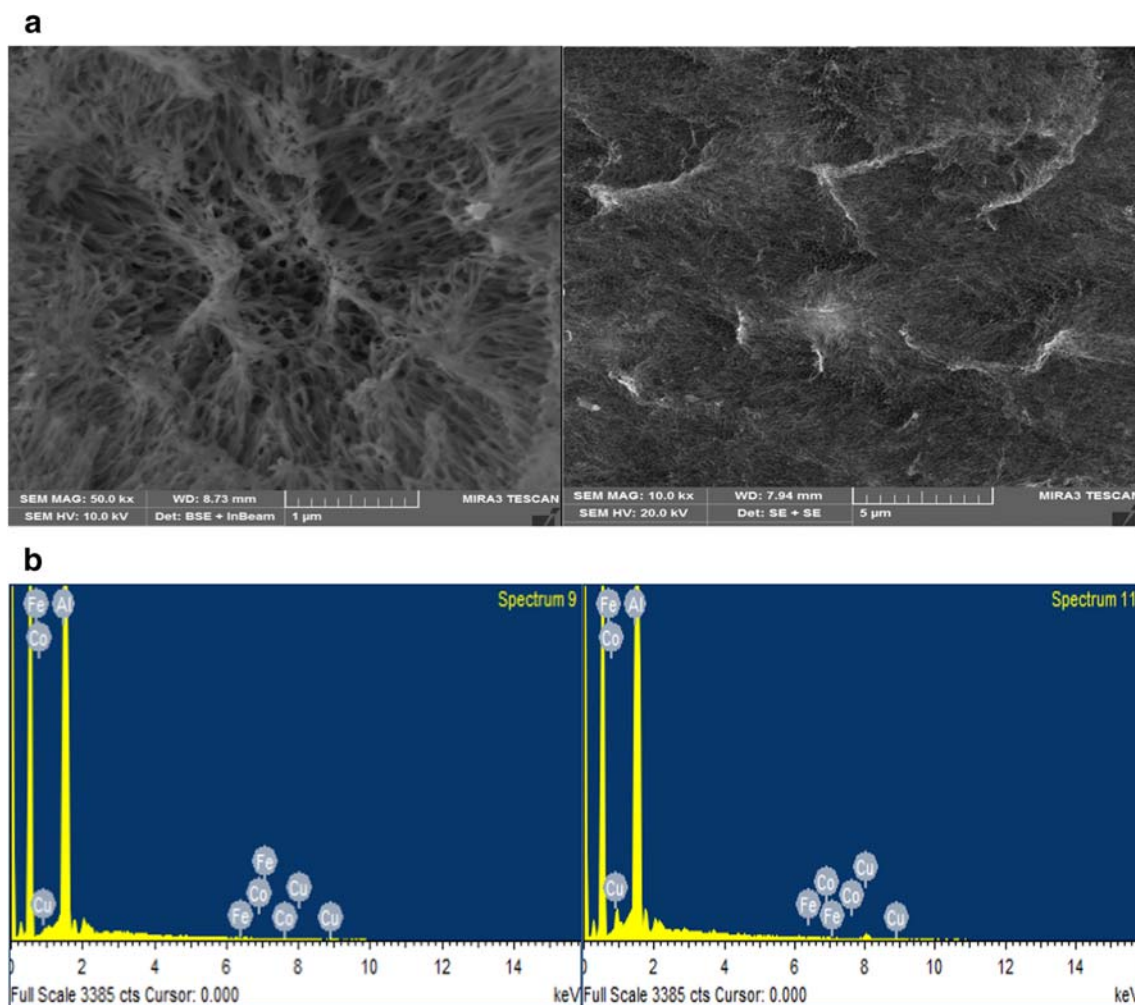


Fig. 1 a SEM image of synthesized FeCoCu NWs (top view). b EDX spectrum of FeCoCu nanowires

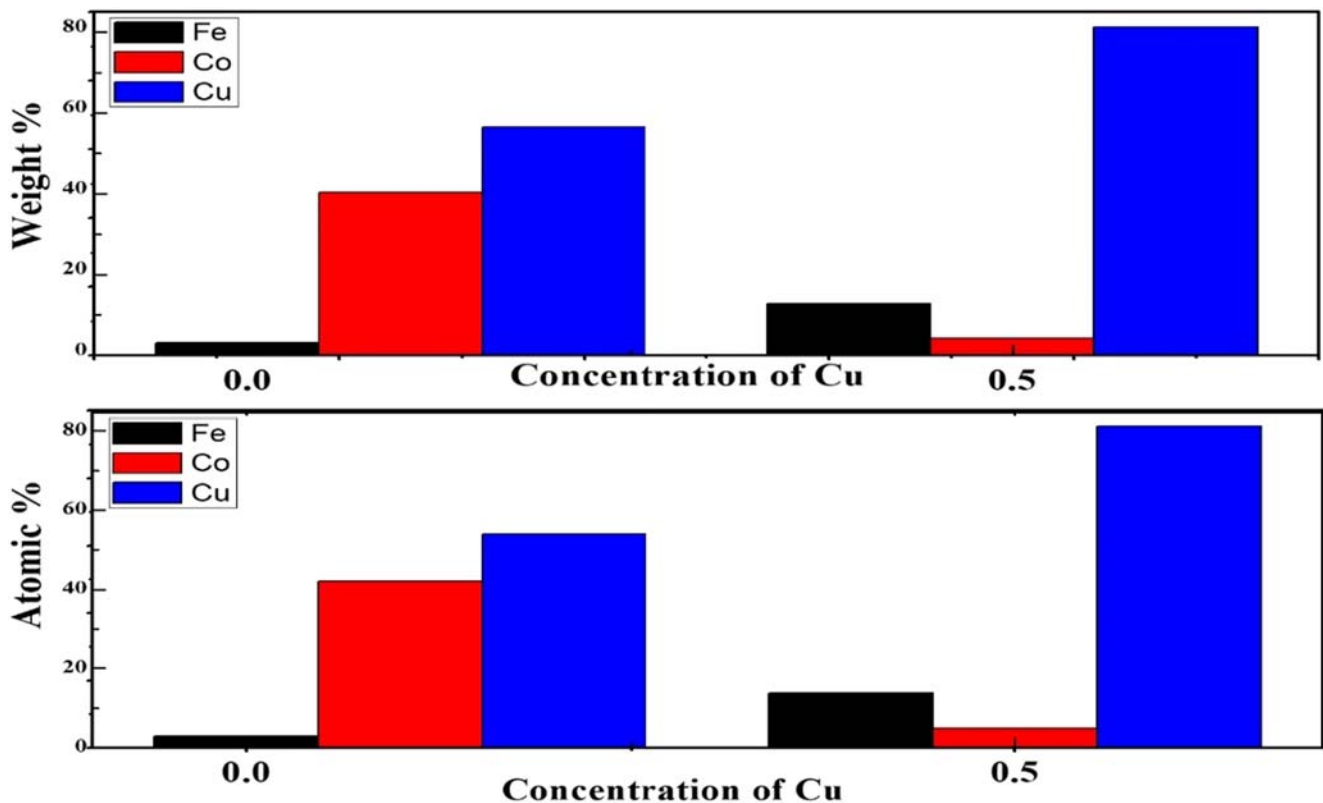


Fig. 2 Compositional pattern of two samples

non-uniformity in pores [13]. After removal of anodization layer, Al sheet was again anodized under same conditions as first anodization for 20 h. At last, the voltage was reduced systematically (1 V/60 s) from 6 to 60 V to breakdown the barrier layer to produce conducting path at the bottom of AAO templates.

2.1.1 Synthesis of $(\text{FeCo})_{1-x}\text{Cu}_x$ ($x = 0-0.5$) Nanowires

After successful fabrication of AAO templates, FeCoCu alloy NWs were synthesized through AC-electrochemically deposition into the pores through electrolyte solution containing 0.3 M $\text{CoSO}_4 \cdot 7\text{H}_2\text{O}$, 0.2 M $\text{FeSO}_4 \cdot 7\text{H}_2\text{O}$, and varying the concentration of $\text{CuSO}_4 \cdot 6\text{H}_2\text{O}$ start from 0 M, 0.1 M, 0.2 M, 0.3 M, 0.4 M, and 0.5 M to synthesize six different concentration (FeCoCu alloy NWs) samples. And 0.1 M H_3BO_3 and 0.1 M $\text{CH}_3(\text{CH}_2)_{11}\text{SO}_4\text{Na}$ were also added as buffering and complexing agents, respectively. All six samples were synthesized at 15 V for 60 s with pH = 4.

3 Results and Discussion

3.1 Scanning Electron Microscopy (SEM)

The morphology of FeCoCu NWs is characterized through scanning electron microscope (SEM). For such analysis, first,

the samples were dipped into 0.0125 M NaOH solution to remove the template from FeCoCu NWs. SEM images of FeCoCu NWs prepared at different concentration of Cu are shown in Fig. 1a.

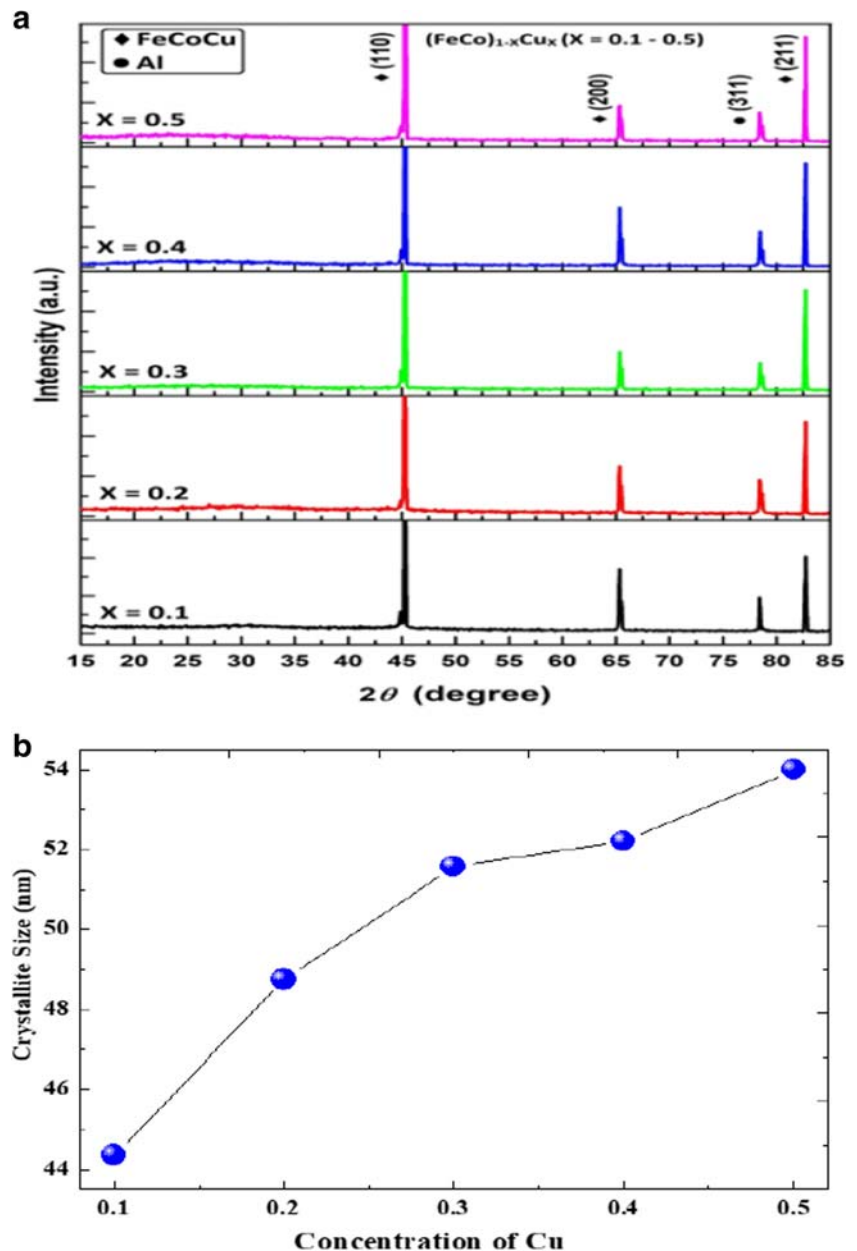
The SEM results show the morphology of the FeCoCu alloy NWs confirming that the diameter of the NWs is in the range of 50–60 nm. The SEM shows that all the pores of anodic alumina template are filled.

3.2 Elemental Composition Analysis

The energy dispersive spectroscopy (EDS) was used to examine chemical composition of FeCoCu NWs. Energy dispersive spectroscopy is a powerful tool to find out the quantity of the material in a sample. EDS confirms the deposition of FeCoCu NWs and shows the presence of Fe, Co, and Cu in AAO template as shown in Fig. 1b.

The Al peak observed in EDX spectra is due to the presence of AAO template, and different peaks of Fe, Co, and Cu are related to our magnetic NWs. The weight and atomic percentage are given only of two samples (first and last), to illustrate the variation of Fe, Co, and Cu concentrations in the deposited NWs (FeCoCu) as shown in Fig. 2. It is observed that as we increase the Cu concentration (from 0 to 0.5 M) in the electrolyte solution, concentration of Cu in the deposited NWs (FeCoCu) shows increasing trend compared with Fe and Co as illustrated in Fig. 2.

Fig. 3 a XRD pattern of FeCoCu nanowires. b Concentration dependent crystallite size



3.3 Structural Analysis

The XRD pattern is a graphical representation which is used for structural analysis of the material. The $(\text{FeCo})_{1-x}\text{Cu}_x$ ($X = 0.1$ –

Table 1 Crystallite size of nanowires with concentration of Cu

Sample composition	Crystallite size (nm)
$X = 0.1$	44.35
$X = 0.2$	48.75
$X = 0.3$	51.75
$X = 0.4$	53
$X = 0.5$	54

0.5) NWs arrays were characterized through XRD inside the AAO templates as shown in Fig. 3a. The indexed peaks of FeCoCu NWs at (110), (220), and (211) planes correspond to the diffraction angles at $2\theta = 45.25^\circ$, 65.1° , and 81.7° respectively. The indexed peaks at (200) represent the miller indices of diffraction plane corresponding to the diffraction angle $2\theta = 78.2^\circ$ for Al. The AAO templates seem to be amorphous, whereas the FeCoCu NWs have BCC phase (PDF2 Card No. 44-1433) along with Al FCC extra phase of substrate, and the average crystalline size of NWs is calculated from X-ray diffraction peaks by using Scherer's equation as given in Eq. 1 [19]:

$$\langle D_{\text{XRD}} \rangle = \frac{k\lambda}{\beta \cos\theta} \quad (1)$$

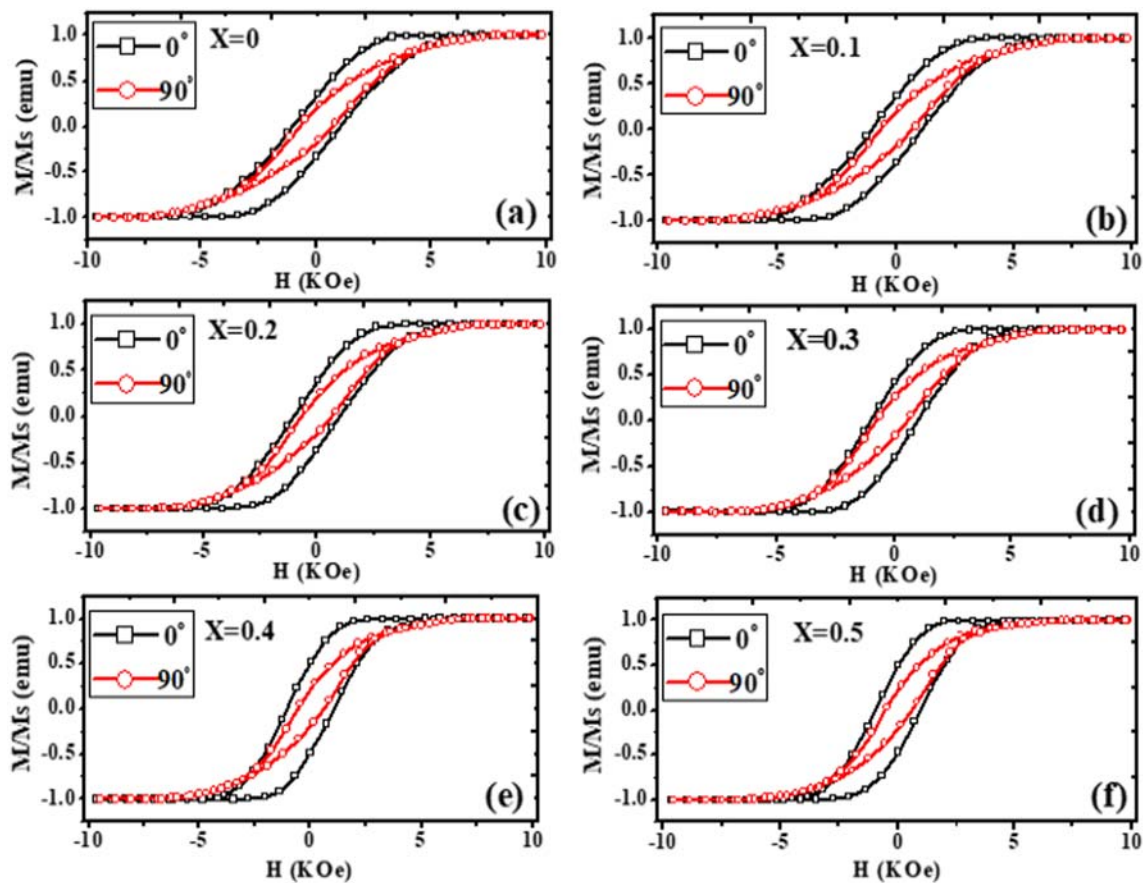


Fig. 4 M-H curves of FeCoCu nanowires at different concentrations of Cu

where D shows the average grain size, k is the Scherrer constant also known as crystallite shape factor equal to 0.89 for NWs, λ is the wavelength of X-rays having Cu-K α line equal to 0.154 nm falling on NWs, β is the full width at half maximum (FWHM) of diffraction peak (110) of X-ray, and θ is the diffracted angle. The crystallite size of NWs varies from 44 to 54 nm calculated by Scherer’s equation. When the concentration of Cu increases, the crystallite size of FeCoCu NWs also increases because the ionic radii of Cu are greater than that of Fe and Co. The change in crystallite size by varying the concentration of Cu is shown in Table 1 and Fig. 3b.

3.4 Magnetic Properties

Vibrating sample magnetometer was used to measure the magnetic properties of (FeCo) $_{1-x}$ Cu $_x$ ($X = 0.1–0.5$) NWs. We have done basic magnetic characterization such as M-H loop along 0° and 90° (parallel and perpendicular to the NWs), respectively, and they exhibit anisotropic behavior of magnetization and coercivity at two angles as shown in Fig. 4.

Figure 4 shows ferromagnetic behavior because Fe and Co are strong magnetic materials. Magnetization and coercivity decreases by increasing the composition of Cu in FeCoCu NWs due to nonmagnetic behavior of Cu. As earlier described, Fe and

Co are ferromagnetic materials having large saturation magnetization (M_s) and coercivity (H_c); on the other hand, Cu is diamagnetic or nonmagnetic material. Squareness (M_r/M_s) increases and coercivity decreases by increasing concentration of Cu when magnetic field is applied parallel and perpendicular to the NWs as shown in Fig. 5a–b. Addition of Cu ions may introduce internal stresses, reduction in axial anisotropy, and depinning of domain walls causing a decrease of H_c .

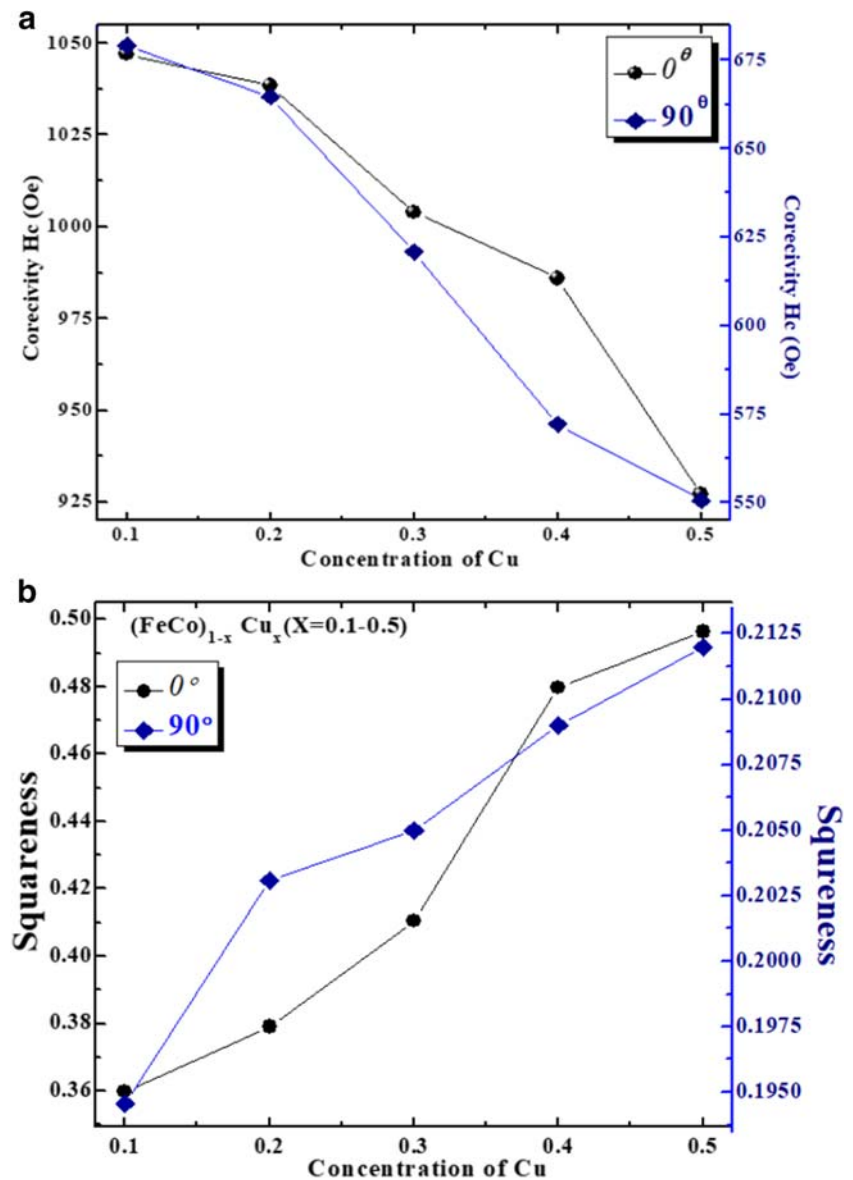
We examined that small coercivity H_C , large saturation field, and a small remanence M_r along the NWs, contrarily H_C , and M_r become larger, and M_s becomes smaller perpendicular to NWs. Hence, this indicates that the easy axis lies along the NWs, and hard axis is perpendicular to the NWs. This is a characteristic of polycrystalline wires where the shape anisotropy dominates over the intrinsic magneto crystalline anisotropy as earlier reported in literature [19].

The effective anisotropy is also defined by the following equation:

$$H_K = 2\pi M_S - 6.3\pi M_S r^2 L / D^3 + H_{ma} \tag{2}$$

The 1st term of Eq. (2) illustrates the behavior of the shape anisotropy and it tries to align the magnetic moments parallel (easy axis) to the NWs. The 2nd term shows the dipole-dipole interactions called magnetostatic interactions that try to align

Fig. 5 a Coercivity of FeCoCu nanowires with concentration of Cu at $\theta = 0^\circ$ and 90° . b Squareness of FeCoCu nanowires with concentration of Cu at $\theta = 0^\circ$ and 90°



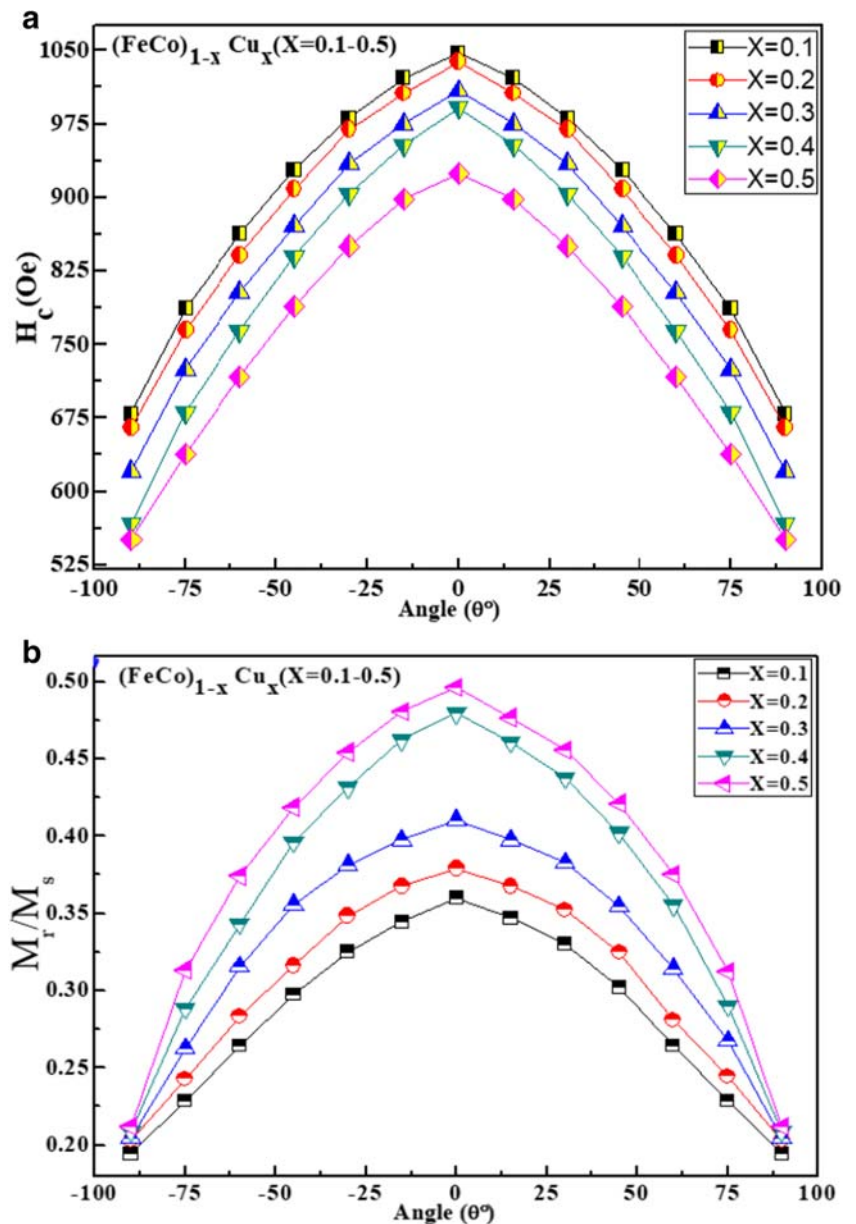
the magnetic moment perpendicular (hard axis) to the NWs, and the 3rd term displays magneto-crystalline anisotropy. In NWs, the shape anisotropy is dominated which effect to enhance the squareness along (easy axis) the NWs, and diminished to the perpendicular of the NWs [20].

The easy axis is also determined from equation $\Delta H_s = H_{s\parallel} - H_{s\perp}$ as shown in Table 2 where $H_{s\parallel}$ is saturation field when magnetic field is applied along the axis of nanowires and $H_{s\perp}$ saturation field when magnetic field is applied perpendicular to the axis of nanowires. The negative value of

Table 2 Magnetic properties of FeCoCu nanowires

Sample detail	Coercivity (Oe)		Mr (emu/g)		Ms (emu/g)		Mr/Ms		$\Delta H_s = H_{s\parallel} - H_{s\perp}$ (Oe)
	\parallel	\perp	\parallel E-3	\perp E-3	\parallel E-3	\perp E-3	\parallel	\perp	
Cu = 0.1	1047	679	3.298	2.0342	9.167	10.45	0.359	0.194	-3222
Cu = 0.2	1038	664.65	1.918	1.0471	5.064	5.156	0.378	0.203	-3066
Cu = 0.3	1004	620.84	1.779	0.9576	4.335	4.654	0.410	0.205	-2584
Cu = 0.4	995	566.77	1.461	0.5895	3.045	2.813	0.479	0.209	-2578
Cu = 0.5	927	550.68	1.294	0.7981	2.608	3.755	0.496	0.212	-1939

Fig. 6 a Angular dependence of coercivity. b Angle-dependent squareness

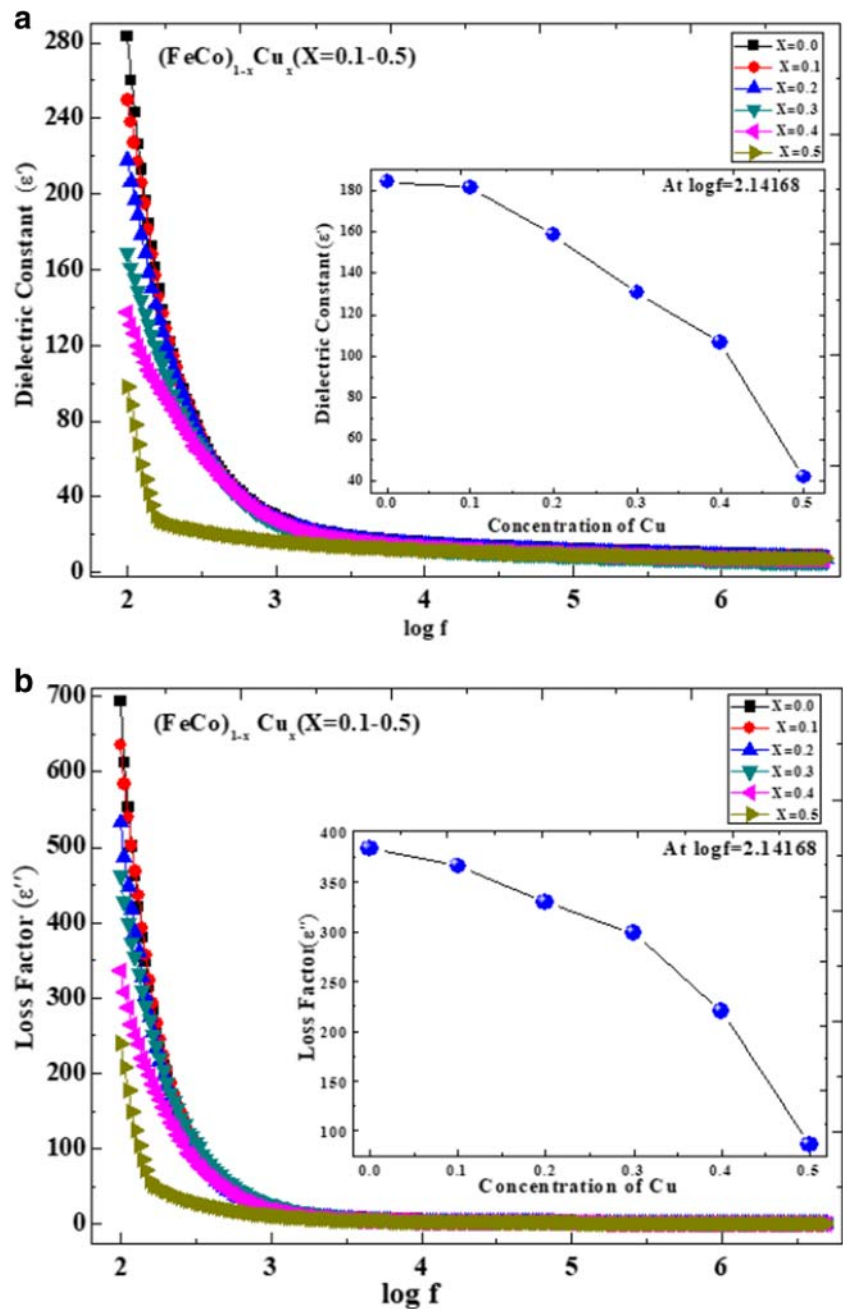


ΔH_s also confirms that easy axis is parallel to nanowire axis. The first term in Eq. (2) describes about shape anisotropy which becomes dominant if ΔH_s is negative. The reduction of ΔH_s with the increase of Cu is linked with saturation magnetization which is also decreasing due to diamagnetic nature of copper.

In case of NWs to be used in magnetic devices, the magnetization reversal (MR) mechanism plays a vital role which is observed from the coercivity with respect to the angle between applied magnetic field and the axis of NWs. If a magnetic NW is placed in the external magnetic field, the magnetic moments inside the NW try to align themselves along the external magnetic field. In literature, so many possible reversal mechanisms have been explained

such as nucleation, curling, buckling, and coherent mode. An easy approach to explain the reversal mechanism precisely is the coercivity changes with respect to the angle between the NWs and external magnetic field. In coherent mode, coercivity (H_c) decreases with increase of angle; and in curling mode, coercivity (H_c) increases with the increase of angle. For coherent mode of magnetization reversal, coherence length or domain wall width should be equivalent to the length of NWs. The domain walls are nucleated at some position in NWs and then travel from one position to another inside the NWs is known as nucleation mode. In our samples, nucleation mode occurs as H_c is maximum and minimum at $\theta = 0^\circ$ and 90° , respectively, from angular dependence of coercivity as shown in Fig. 6a, and

Fig. 7 a Dielectric constant of $(\text{FeCo})_{1-x}\text{Cu}_x$ ($X=0.1-0.5$) nanowires. Inset shows the variation of real parts with Cu concentration (x). b Imaginary part of dielectric constant of $(\text{FeCo})_{1-x}\text{Cu}_x$ ($X=0.1-0.5$) nanowires. Inset shows the variation of imaginary parts with Cu concentration (x)



squareness (ratio of remanence and saturation magnetization known as squareness) of FeCoCu NWs is shown in Fig. 6b.

3.5 Dielectric Properties

Before the start of characterization of FeCoCu alloy NWs through LCR meter for dielectric properties, first, the samples were dipped in the 0.0125 M NaOH aqueous solution for 1 h at 60 °C, through which templates (work as insulator) were removed from the upper part of NWs while in the lower remained there to support the NWs in the standing mode

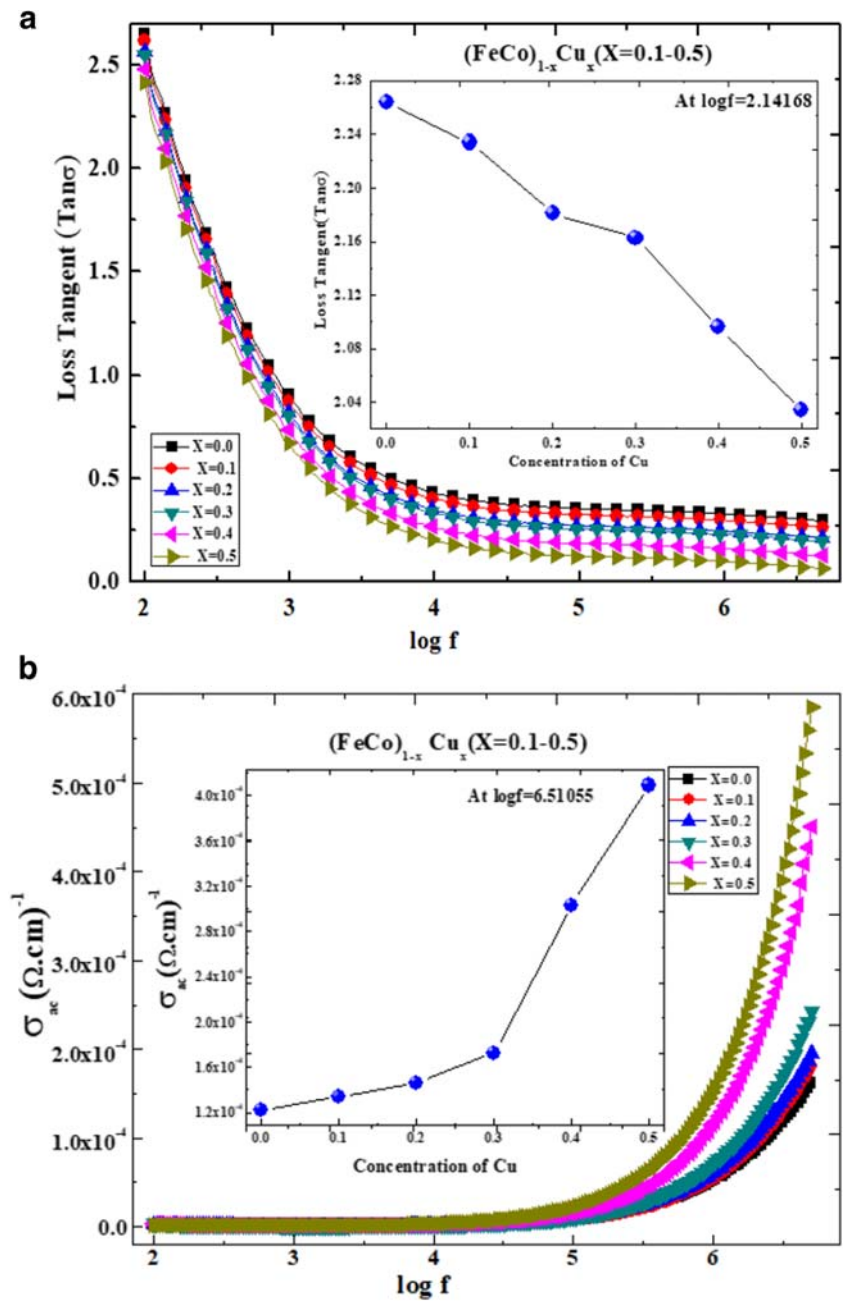
and produced no hurdle during the characterizations. Then electrodes were connected to the copper plates.

Materials that have ability to store energy when electric field is applied to them are called dielectric materials. The dielectric constant is measured by the following relation:

$$\epsilon' = \frac{Cd}{\epsilon_0 A} \quad (3)$$

where C is capacitance, d is thickness of the sample, ϵ_0 is permittivity, and A is the area of cross section and the imaginary part of dielectric constant is measured by the following relation:

Fig. 8 a Frequency dependence of tangent loss for $(\text{FeCo})_{1-x}\text{Cu}_x$ ($X=0.1-0.5$) nanowires. b Frequency dependence of conductivity for $(\text{FeCo})_{1-x}\text{Cu}_x$ ($X=0.1-0.5$) nanowires



$$\mathcal{E}'' = \mathcal{E}' \tan\delta \tag{4}$$

The dielectric properties of materials depend on crystal structure, grain size, frequency of applied field, cation distribution and temperature, etc. Frequency-dependent dielectric properties of $(\text{FeCo})_{1-x}\text{Cu}_x$ ($X=0.1-0.5$) NWs were measured in the frequency range from 100 Hz to 5 MHz at ambient temperature. The real part (\mathcal{E}') and imaginary (\mathcal{E}'') part of dielectric constant are shown in Fig. 7a and b, respectively. Both \mathcal{E}' and \mathcal{E}'' have confirmed the highest values at low frequencies and declined at higher frequencies. It is the typical behavior of dielectric constant attributed to interfacial/space

charge polarization due to nonuniform microstructure as well as mismatch in exchange interaction of the electron which cannot withstand the high alternating electric field with the change of frequency. Our sample is termed as a heterogeneous material, which has a granular nature and contains pores. Pores and grains inside the material make prominent due to the effect of interfacial/space charge polarization. This effect is known as Maxwell-Wagner effect or M-W effect. Dielectric material contained grains and grain boundaries according to M-W effect. The grains act as a conducting region, and grain boundaries act as a resistive region. The electrons approach to the grain boundaries by hopping phenomena. Due to the

highly resistive nature of the grain boundaries, electrons are stacked and produce polarization [20]. The value of dielectric constant decreases progressively with increasing frequency [21] and vice versa. It is also observed that with increase in Cu concentration, the dielectric constant also decreases. The degree of polarization decreases due to modification in structural homogeneity caused by variation of Cu for Co. Dielectric constant decreases because Cu has higher conductivity ($5.95 \times 10^{-7} \Omega/\text{m}$) than Fe ($1 \times 10^{-7} \Omega/\text{m}$) and Co ($1.7 \times 10^{-7} \Omega/\text{m}$) as shown in Fig. 7b. At lower frequencies, the polarization effect is due to the interfacial and dipolar polarization while at higher frequencies, electronic polarization plays its role.

The power loss is defined as the loss tangent or $\tan \delta$ and written as follows:

$$\tan \delta = \frac{1}{2\pi f C_p R_p} \quad (5)$$

where R_p and C_p are the parallel resistance and parallel capacitance, respectively. The loss factor determines the loss in the material due to the damping of the dipoles moments vibrating inside a material. Figure 8a shows that the $(\text{FeCo})_{1-x}\text{Cu}_x$ ($X=0.1-0.5$) NWs at room temperature show the variation of tangent loss w.r.t frequency. Tangent loss shows highest value at low frequency because of the capability of minimum charge storage. The disparity of tangent loss as a function of frequency can be clarified through Maxwell model [22–24].

The loss factor and tangent loss are very significant in defining the properties of the materials used in engineering. Electronics industry requires materials which show good electrical performance and are cost effective. Examples include testing instruments, oscilloscopes, and desktop computers which need fast signal processing methods. The AC conductivity is calculated by the following formula:

$$\sigma_{ac} = 2\pi f \varepsilon_0 \varepsilon' \tan(\delta) \quad (6)$$

AC conductivity at lower frequency shows small values and at higher frequency values shows large value which is a normal trend. AC conductivity increased by increasing concentration of Cu as shown in Fig. 8b. Since copper is a conductive material, the increase in concentration of copper in FeCoCu nanowires will increase AC conductivity [25, 26].

4 Conclusion

The $(\text{FeCo})_{1-x}\text{Cu}_x$ NWs arrays with different Cu concentrations were synthesized through AC- electrochemical deposition embedded inside the self-assembled AAO templates. The structure of the NWs has been investigated inside AAO templates. Microstructures, dielectric, and magnetic properties of the nanowires were observed and led to the interesting results.

The average crystallite size was found by Scherrer's equation, lies in the range 44–54 nm for different Cu contents of FeCoCu NWs. The crystallite size exhibited an increasing trend with Cu content, and BCC crystalline structure of FeCoCu NWs is confirmed by X-rays analysis. The Cu composition of NWs increased as compared with Fe and Co atoms during the AC electrodeposition process observed by EDS analysis. The diameter of the NWs is in the range of 50–60 nm confirmed by SEM analysis. The increase in Cu concentration resulted in reduction of the magnetization and coercivity of the FeCoCu nanowires. Magnetization reversal shows the nucleation mode of magnetization with motion of domain walls. The coercivity and squareness both were decreased w.r.t increase of angle and display their maximum value parallel (0°) to the NWs and minimum value perpendicular (90°) to the NWs. The study of dielectric such as the tangent loss, dielectric loss and dielectric constant was decreased w.r.t increase of frequency attributed to interfacial/space charge polarization due to nonuniform microstructure. It is also concluded that with increase of Cu content, the maximum value of tangent loss, dielectric loss, and dielectric constant decreases opposite to that of AC-conductivity due to higher concentration of copper. This study shows that magnetic and dielectric properties of the FeCoCu nanowires inside AAO templates can be tuned according to our own desire depending upon specific applications.

Funding information This project is supported by Higher Education Commission, Pakistan, by Pakistan through Pakistan Programme for Collaborative Research (PPCR).

References

1. Al-Mawlawi, D., Liu, C.Z., Moskovits, M.: Nanowires formed in anodic oxide nanotemplates. *J. Mater. Res.* **04**, 1014–1018 (1994)
2. Wäckelgård, E.: A study of the optical properties of nickel-pigmented anodic alumina in the infrared region. *J. Phys. Condens. Matter.* **8**, 5125 (1996)
3. Fodor, P.S., Tsoi, G.M., Wenger, L.E.: Fabrication and characterization of $\text{Co}_{1-x}\text{Fe}_x$ alloy nanowires. *J. Appl. Phys.* **10**, 8186–8188 (2002)
4. Avella, M., Cocca, M., Errico, M.E., Gentile, G.: Nanotechnologies and nanosensors: future applications for the conservation of cultural heritage. *Nanotechnol. Basis Adv. Sensors.* **3**, 511–517 (2011)
5. Ramazani, A., Almasi-Kashi, M., Golafshan, E., Arefpour, M.: Magnetic behavior of as-deposited and annealed CoFe and CoFeCu nanowire arrays by ac-pulse electrodeposition. *J. Cryst. Growth.* **402**, 42–47 (2014)
6. Darques, M., De la Torre Medina, J., Piraux, L., Cagnon, L., Huynen, I.: Microwave circulator based on ferromagnetic nanowires in an alumina template. *Nanotechnology.* **14**, 145208 (2010)
7. Saavedra, E., Saez, G., Díaz, P., Cisternas, E., Vogel, E.E., Escrig, J.: Dynamic susceptibility of modulated magnetic nanowires. *AIP Adv.* **9**, 065007 (2019)
8. Berganza, E., Bran, C., Jaafar, M., Vázquez, M., Asenjo, A.: Domain wall pinning in FeCoCu bamboo-like nanowires. *Sci. Rep.* **6**, 29702 (2017)

9. Fodor, P.S., Tsoi, G.M., Wenger, L.E.: Fabrication and characterization of $\text{Co}_{1-x}\text{Fe}_x$ alloy nanowires. *J. Appl. Phys.* **10**, 8186–8188 (2002)
10. Wang, R.L., Tang, S.L., Shi, Y.G., Fei, X.L., Nie, B., Du, Y.W.: Effects of annealing on the structure and magnetic properties of $\text{Fe}_{27}\text{Co}_{23}\text{Pb}_{50}$ nanowire arrays. *J. Appl. Phys.* **103**, 07D507 (2008)
11. Shukla, G.: Magnetic and optical properties of epitaxial n-type Cu-doped ZnO thin films deposited on sapphire substrates. *Appl. Phys. A Mater. Sci. Process.* **1**(115–118), (2009)
12. Guo, Y., Qin, D.-H., Ding, J.-B., Li, H.-L.: Annealing and morphology effects on the Fe 0.39 Co 0.61 nanowire arrays. *Appl. Surf. Sci.* **218**, 107–113 (2003)
13. Khan, S., Ahmad, N., Ahmed, N., Safeer, A., Iqbal, J., Han, X.F.: Structural, magnetic and transport properties of Fe-based full Heusler alloy Fe_2CoSn nanowires prepared by template-based electrodeposition. *J. Magn. Magn. Mater.* **465**, 462–470 (2018)
14. Khan, S., Ahmad, N., Safeer, A., Iqbal, J.: Compositional dependent morphology, structural and magnetic properties of $\text{Fe}_{100-x}\text{Cu}_x$ alloy nanowires via electrodeposition in AAO templates. *Appl. Phys. A.* **678**, 124 (2018)
15. Laocharoensuk, R., Bulbareello, A., Mannino, S., Wang, J.: Adaptive nanowire–nanotube bioelectronic system for on-demand bioelectrocatalytic transformations. *Chem. Commun.* **32**, 3362–3364 (2007)
16. Palmero, E.M., Bran, C., Rafael, P., Magén, C., Vázquez, M.: Structural and magnetic characterization of FeCoCu/Cu multilayer nanowire arrays. *IEEE Magn. Lett.* **5**, 1–4 (2014)
17. Ahmad, N., Chen, J.Y., Iqbal, J., Wang, W.X., Zhou, W.P., Han, X.F.: Temperature dependent magnetic properties of Co nanowires and nanotubes prepared by electrodeposition method. *J. Appl. Phys.* **109**, 07A331 (2011)
18. Méndez, M., González, S., Vega, V., Teixeira, J.M., Hernando, B., Luna, C., Prida, V.M.: Ni-Co alloy and multisegmented Ni/Co nanowire arrays modulated in composition: structural characterization and magnetic properties. *Crystals.* **7**, 66 (2017)
19. Bran, C., Ivanov, Y.P., García, J., Del Real, R.P., Prida, V.M., Chubykalo-Fesenko, O., Vázquez, M.: Tuning the magnetization reversal process of FeCoCu nanowire arrays by thermal annealing. *J. Appl. Phys.* **114**, 043908 (2013)
20. Han, G.C., Zong, B.Y., Luo, P.: Angular dependence of the coercivity and remanence of ferromagnetic nanowire arrays. *J. Appl. Phys.* **93**, 11 (2003)
21. Kumar, G., et al.: Electric and dielectric study of cobalt substituted Mg-Mn nanoferrites synthesized by solution combustion technique. *Ceram. Int.* **39**(5), 4813–4818 (2013)
22. Mazen, S., Mansour, S., Zaki, H.: Some physical and magnetic properties of Mg-Zn ferrite. *Cryst. Res. Technol.* **38**(6), 471–478 (2003)
23. Kharabe, R., et al.: Dielectric properties of mixed Li–Ni–Cd ferrites. *Smart Mater. Struct.* **15**(2), N36 (2006)
24. Mazen, S., Zaki, H.: Effect of tetra ionic substitution on the dielectric properties of Cu-ferrite. *Phys. Status Solidi A.* **199**(2), 305–320 (2003)
25. Mazen, S.: Infrared absorption and dielectric properties of Li–Cu ferrite. *Mater. Chem. Phys.* **62**(2), 139–147 (2000)
26. Núñez, A., Pérez, L., Abuín, M., Araujo, J.P., Proenca, M.P.: Magnetic behaviour of multisegmented FeCoCu/Cu electrodeposited nanowires. *Phys. D Appl. Phys.* **50**, 155003 (2017)

Publisher's note Springer Nature remains neutral with regard to jurisdictional claims in published maps and institutional affiliations.